https://doi.org/10.47183/mes.2025-396

COMPUTATIONAL PHANTOM FOR RED BONE MARROW DOSIMETRY IN 15-YEAR-OLD ADOLESCENTS

Pavel A. Sharagin[1]✉, Evgenia I. Tolstykh[1], Elena A. Shishkina[1,2]

[1] Southern Urals Federal Research and Clinical Center for Medical Biophysics, Ozersk, Russia
[2] Chelyabinsk State University, Chelyabinsk, Russia

Introduction. Computational phantoms are widely used for assessing radiation doses to the red bone marrow (RBM) from bone-seeking radionuclides. Among them, strontium isotopes are the most common. The development of phantoms for ^{89,90}Sr requires accurate description of bone shape, size, and microarchitecture. To date, phantoms for newborns, one-year-old, five-year-old, and 10-year-old children, as well as for adult males and females, have been proposed. This study is a continuation of our work on creating digital skeletal models for humans of different sexes and ages.
Objective. Development of computational phantoms for the skeleton for 15-year-old adolescents with the purpose of assessing doses in RBM from incorporated beta-emitting radionuclides.
Materials and methods. The phantoms were developed using the stochastic parametric skeletal dosimetry (SPSD) approach. Skeletal regions with active hematopoiesis were identified and segmented. The parameters of the segment models were estimated based on literature data, including bone microstructural characteristics, cortical bone layer thickness, bone and segment dimensions, the fractional content of RBM, and the chemical composition and density of the modeled media. The variability ranges of these parameters were also assessed.
Results. The developed phantoms for 15-year-old male and female adolescents comprise 46 segments each; parameters for 14 of these segments differed between males and females. The phantom dimensions ranged 3.5–66 mm; the cortical bone thickness varied 0.3–2.3 mm.
Conclusions. The phantoms developed in this work reflect the dimensions and structure of skeletal regions with active hematopoiesis in 15-year-old adolescents, account for sexual dimorphism, and simulate the variability of skeletal characteristics.

Keywords: trabecular bone; cortical bone; bone marrow dosimetry; computational phantoms; strontium

For citation: Sharagin P.A., Tolstykh E.I., Shishkina E.A. Computational phantom for red bone marrow dosimetry in 15-year-old adolescents. *Extreme Medicine.* 2026;28(2):205–214. https://doi.org/10.47183/mes.2025-396

Funding: this work was supported by a grant of the Russian Science Foundation entitled “Conducting fundamental scientific research and exploratory scientific research by small individual scientific groups” — Regional Competition (Agreement No. 25-25-20092), supported by the Chelyabinsk Region within the program “Science Development in the Chelyabinsk Region”, grant as a subsidy (Agreement No. 30-2025-003346).

Potential conflict of interest: the authors declare no conflict of interest.

✉ Pavel A. Sharagin sharagin@urcrm.ru

Received: 08 Sept. 2025 **Revised:** 21 Oct. 2025 **Accepted:** 14 Nov.2025 **Online first:** 27 Dec. 2025

УДК 614.876

ВЫЧИСЛИТЕЛЬНЫЙ ФАНТОМ ДЛЯ ДОЗИМЕТРИИ КРАСНОГО КОСТНОГО МОЗГА ДЛЯ 15-ЛЕТНИХ ЮНОШЕЙ И ДЕВУШЕК

П.А. Шарагин[1]✉, Е.И. Толстых[1], Е.А. Шишкина[1,2]

[1] Южно-Уральский федеральный научно-клинический центр медицинской биофизики Федерального медико-биологического агентства, Озерск, Россия
[2] Челябинский государственный университет, Челябинск, Россия

Введение. Вычислительные фантомы широко применяются для оценки доз облучения красного костного мозга от остеотропных радионуклидов. Наиболее распространенными такими радионуклидами являются изотопы стронция. Создание фантомов для ^{89,90}Sr требует аккуратного описания формы, размеров и микроархитектуры костей. На сегодняшний день опубликованы описания фантомов новорожденного, годовалого, 5-летних и 10-летних детей, а также взрослых мужчины и женщины. Данное исследование является продолжением работы по созданию цифровых моделей скелета для людей разного пола и возраста.
Цель. Разработка вычислительных фантомов скелетов 15-летних юношей и девушек для оценки доз в красном костном мозге (ККМ) от инкорпорированных бета-излучающих радионуклидов.
Материалы и методы. Для создания фантомов был использован SPSD (stochastic parametric skeletal dosimetry) подход. Были выделены участки скелета с активным гемопоэзом, которые были разделены на сегменты. Параметры моделей сегментов были оценены по данным литературы и включали в себя: характеристики микроструктуры кости, толщину слоя кортикальной кости, размеры костей и их участков, а также долю содержания ККМ, химический состав и плотность моделируемых сред. Также были оценены значения вариабельности этих параметров.
Результаты. Разработанные фантомы 15-летних юношей и девушек включают по 46 сегментов; параметры 14 из них различались для юношей и девушек. Размеры фантомов были 3,5–66 мм, а толщина кортикальной кости 0,3–2,3 мм.
Выводы. Фантомы, полученные в рамках данной работы, отражают размеры и структуру участков скелета с активным гемопоэзом 15-летних юношей и девушек, учитывают половые различия, а также имитируют вариабельность характеристик скелета.

Ключевые слова: трабекулярная кость; кортикальная кость; дозиметрия костного мозга; вычислительные фантомы; стронций

Для цитирования: Шарагин П.А., Толстых Е.И., Шишкина Е.А. Вычислительный фантом для дозиметрии красного костного мозга для 15-летних юношей и девушек. *Экстремальная биомедицина*. 2026;28(2):205–214. https://doi.org/10.47183/mes.2025-396

Финансирование: работа выполнена в рамках гранта Российского научного фонда по мероприятию «Проведение фундаментальных научных исследований и поисковых научных исследований малыми отдельными научными группами» (региональный конкурс) Соглашение № 25-25-20092 поддерживаемое регионом, — программа Челябинской области «Развитие науки в Челябинской области», грант в форме субсидии (Соглашение № 30-2025-003346).

Потенциальный конфликт интересов: авторы заявляют об отсутствии конфликта интересов.

✉ Шарагин Павел Алексеевич sharagin@urcrm.ru

Статья поступила: 08.09.2025 **После доработки:** 21.10.2025 **Принята к публикации:** 14.11.2025 **Online first:** 27.12.2025

INTRODUCTION

Assessment of doses from incorporated bone-seeking radionuclides plays an essential role in predicting radiogenic risks for individuals residing in contaminated areas. Strontium isotopes are among the most common of these radionuclides, which can be released into the environment both through global fallout and other technogenic radiation incidents. ^{90}Sr is a long-lived, bone-seeking, beta-emitting radionuclide; its accumulation in bone tissue leads to chronic irradiation of the red bone marrow (RBM), thereby increasing the risk of developing leukemia [1–4].

Assessment of doses from strontium isotopes involves the use of biokinetic and dosimetric models. A biokinetic model was previously developed at the Ural Scientific and Practical Center for Radiation Medicine (Russia).[1] This model simulates the transport processes of Sr within the body; the output of this model is the specific activity of Sr in bone tissue. The dosimetric model enables calculation of dose conversion factors (DF) from the specific activity of the radionuclide in bone tissue to the absorbed dose rate in RBM (Gy/s) [5]. Such models are developed based on the creation of computational phantoms, representing 3D models that simulate the spatial arrangement and composition of media in which radiation transport will subsequently be simulated. Developing such phantoms for beta-emitters is a challenging task due to the necessity of adequately describing both the linear dimensions of bones and their microstructure.

Modern phantoms used for the internal dosimetry of strontium are based on the analysis of medical images of human skeletons[2] [6–10]. Consequently, such phantoms have a significant limitation for their use in cohort studies. Indeed, due to the limited amount of autopsy material, they do not allow for the assessment of uncertainties associated with the variability of skeletal dimensions and microarchitecture within a population.

An alternative approach consists in the parametric method of stochastic modeling of bone structures, referred to as stochastic parametric skeletal dosimetry (SPSD) modeling [11]. This approach, developed at the Ural Scientific and Practical Center for Radiation Medicine (Russia), estimates the phantom parameters based on published bone measurement results rather than using medical images. The extensive body of literature enables assessment of the variability in skeletal characteristics within a population and the associated DF variability.

Previous publications [12–16] were the first to present the parameters of skeletal phantoms for newborns, one-year-old, 5-year-old, and 10-year-old children, as well as for adult males and females. The skeletal regions with active hematopoiesis are identical in 15-year-olds and adults. Furthermore, many skeletal regions in 15-year-old individuals are similar in shape and microstructural characteristics to those in adults. For this reason, phantoms for 15-year-old male and female adolescents were developed based on adult phantoms; in other words, some parameters for 15-year-old phantoms were set equal to those for adults. Similar to adults, sexual dimorphism assessment is also important for 15-year-olds. Thus, this our study represents a new stage in the development of computational phantoms for different age groups.

In this work, we aim to develop computational phantoms of the skeleton for 15-year-old male and female adolescents for assessing doses in RBM from incorporated beta-emitting radionuclides.

MATERIALS AND METHODS

The stages of phantom development did not differ from those for other age groups [11]. The primary stage involved identifying the modeling objects, i.e., skeletal regions with active hematopoiesis, and estimating the mass fraction of RBM in each such a region. Subsequently, linear dimensions and bone microstructural characteristics were estimated based on literature data. Following this, each modeled skeletal region was subdivided into smaller parts. A computational phantom was generated for each such a part.

The RBM mass fraction in various skeletal bones was estimated based on published data [17]. Within the SPSD approach, not the entire skeleton is modeled, but only its regions containing RBM. This rule also applies to individual bones; that is, only their parts containing RBM were modeled. Accordingly, based on MRI study results [18–23], the distribution of RBM within the bones was assessed.

[1] Currently entitled the South Ural Federal Research and Clinical Center for Medical Biophysics.

[2] Pafundi D. Image-based skeletal tissues and electron dosimetry models for the ICRP reference pediatric age series. Dissertation for PhD Degree. University of Florida; 2009.

The phantom parameters for 15-year-old male and female adolescents, similar to those for other age groups, included average values of bone microstructural parameters, i.e., trabecular thickness (*Tb. Th.*), mean trabecular separation (*Tb. Sp.*), and the bone volume fraction (*BV/TV*) [24]. Bone and segment dimensions, as well as cortical bone layer thickness (*Ct. Th.*), were also phantom parameters. We estimated all these parameters based on measurement results obtained using histomorphometry and micro-computed tomography (micro-CT) and published in the respective literature.

Literature data were collected and analyzed according to a previously described methodology [24]. The parameters of the adult male and female phantoms [16] were used for those skeletal regions for which no published data were found. Measurement results from bones of Caucasians and Mongoloids were included in the analysis, given that these ethnic groups are representative of the Ural region for the age range of 13–17 years.

Bone microarchitecture parameters were estimated using the published data obtained by histomorphometry and micro-CT. Cortical bone thickness was assessed based on published measurement results obtained using CT, micro-CT, and micrometer gauges. Linear bone dimensions were estimated from published measurement results utilizing anatomical boxes, ultrasonography, radiographic studies, and CT.

In the absence of sexual dimorphism in the studied bone characteristics, datasets for both sexes were pooled. In such cases, the bone segment was modeled independently of sex. In other instances, phantoms for different sexes were modeled separately.

Each skeletal region with active hematopoiesis was subdivided into smaller parts — segments. All segments feature homogeneous bone microarchitecture and cortical layer thickness and are described by simple geometric shapes [25]. A basic phantom bone segment (BPS) was modeled for each segment. The segmentation was performed such that each segment possessed a homogeneous microarchitecture and a homogeneous cortical layer thickness. For BPSs represented by elongated cylinders or elongated/flat rectangular parallelepipeds, only the portion of BPS whose maximum linear dimensions reached 30 mm was modeled. Further increasing the maximum size of such a BPS does not affect the DF [26]. Thus, segmentation permits accounting for heterogeneous microarchitecture and cortical thickness within a bone, reduces the size of the phantoms (thereby enabling higher resolution), and improves simulation accuracy.

The density and chemical composition of the modeled media (mineralized bone and bone marrow) were identical for all BPSs and were estimated based on literature sources [27, 28]. The generation of BPSs was performed using the Trabecula software application developed in our laboratory [29]. A BPS consists of three media: bone marrow (BM) — the target tissue, as well as cortical bone (CB) and trabecular bone (TB) — two separate source tissues.

Trabecular bone was modeled as a 3D network of bone strands — trabeculae — whose spatial arrangement and thickness were randomly selected within the bounds of bone microarchitecture parameter variability estimated from published data [30–34]. Bone marrow is located in the spaces between the trabeculae, and cortical bone (CB) encases the trabecular bone (TB) externally as a continuous layer with a specified thickness. The voxel size for each BPS was adjusted such that it did not exceed 70% of *Tb. Th.* and ranged within 50–140 μm [29]. The volumes of the media comprising the phantom were calculated in the Trabecula software.

Phantoms created using the SPSD approach enable the assessment of DF uncertainties associated with the variability of skeletal characteristics within a population. For this purpose, sets of supplementary phantoms of bone segment (SPS) were modeled for each BPS. While the BPS was modeled with average parameter values, the parameter values for the SPS were randomly sampled within the boundaries of the minimum and maximum measured values of their variability. The method for uncertainty assessment was described in detail in [35].

Skeletal regions with active hematopoiesis in a 15-year-old adolescent, bone segmentation, and cross-sections of individual segments using the clavicle as an example are presented in the figure.

RESULTS

The set of skeletal regions with active hematopoiesis for 15-year-olds did not differ from that for adults; however, there are differences in the RBM distribution among these regions, as demonstrated in Table 1.

Table 1 shows that the skeleton of 15-year-olds comprises 12 skeletal regions with active hematopoiesis, with the RBM mass fraction ranging 1.0–18.6%. No sexual dimorphism was observed in the RBM distribution within the skeleton.

The elemental composition of the modeled media is equivalent to that in adults [16] and was estimated based on published data [28]. We used the measurement results published for the density of the cortical bone layer in 15-year-olds [27] as the density for both CB and TB (1.85 g/cm^3). The BM density was assumed to be 1.0 g/cm^3 [28].

No significant sexual dimorphism was found in bone microarchitecture characteristics [26]; therefore, data from males and females were pooled. Table 2 presents the microarchitecture parameter values for the BPS of 15-year-old male and female adolescents.

The variability ranges of bone microarchitecture parameters within a bone were used to set the characteristics of the 3D trabecular network model, thereby enhancing its realism. For 15-year-old adolescents, no such variability values were found; therefore, these values were assumed to be the same as for adults [36].

The linear dimensions and cortical layer thickness adopted for the BPS of 15-year-old male and female

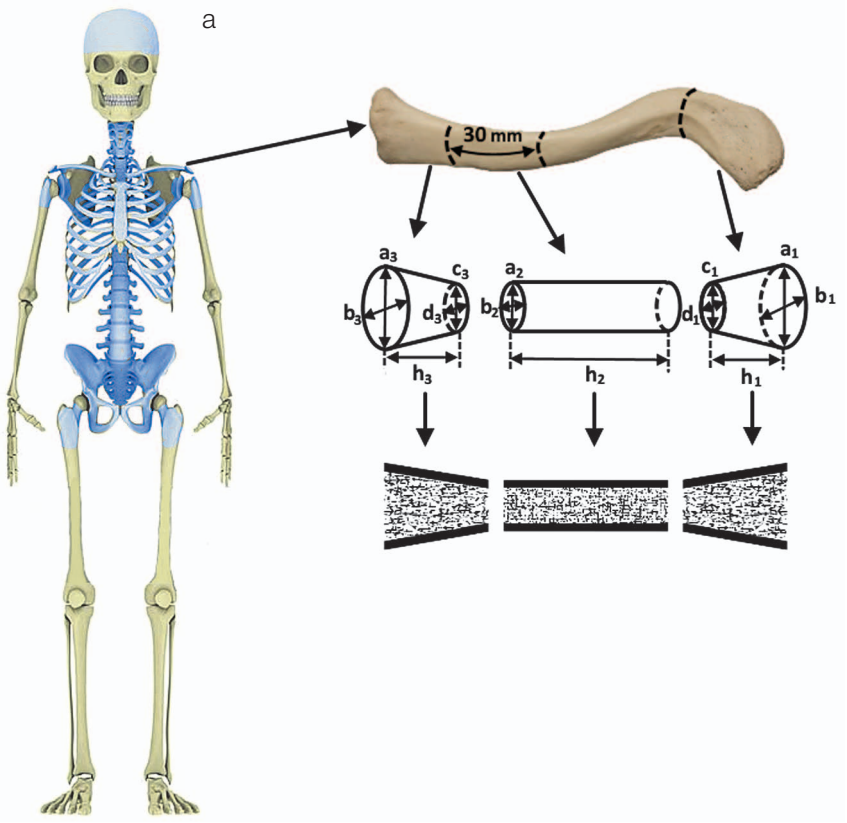

Figure prepared by the authors

Fig. Skeletal regions with active hematopoiesis for a 15-year-old male adolescent and their segmentation illustrated using the clavicle: (a) skeleton of a 15-year-old (regions modeled with active hematopoiesis are highlighted in blue); (b) clavicle (bone segments are outlined by dashed lines); (c) diagram of bone division into basic phantoms of bone segments (BPS) and their linear parameters; (d) BPS of the clavicle in voxel representation, cross section (voxels simulating mineralized bone are shown in black, bone marrow is shown in white)

Table 1. Mass fractions of red bone marrow (RBM) (% of total RBM mass in the skeleton) in the major hematopoietic skeletal sites of 15-year-olds

No.	Hematopoietic site	RBM mass fraction, %	
		15-year-olds	Adults
1	Femur	15.7	5.9
2	Humerus	3.8	3.6
3	Sacrum	8.5	7.4
4	Pelvic bones	18.6	23.2
5	Skull	10.2	6.2
6	Clavicle	1.0	0.8
7	Scapula	3.3	4.7
8	Ribs	13.7	9.8
9	Sternum	1.8	1.8
10	Cervical vertebrae	3.3	3.5
11	Thoracic vertebrae	11.0	17.5
12	Lumbar vertebrae	10.6	15.5

Table prepared by the authors based on data from [19]

Table 2. Bone microarchitecture parameters adopted for the basic phantoms of bone segments of 15-year-old male and female adolescents

Hematopoietic site	*BV/TV*, %	*Tb. Th.*, mm	*Tb. Sp.*, mm
Femur (neck)	35 (23–43)	0.24 (22)	0.54 (14)
Femur trochanter area	26 (17-32)	0.24 (22)	0.54 (14)
Humerus	22 (11–32)	0.21 (13)	0.58 (32)
Ribs	12 (5–25)	0.14 (12)	0.82 (11)
Ilium	25 (20–29)	0.16 (10)	0.46 (0.07)
Ischium bone and pubic ramus inferior	25 (20–29)	0.16 (10)	0.75 (9)
Skull	52 (41–65)	0.29 (32)	0.57 (35)
Clavicle body	15 (10–20)	0.2 (32)	0.8 (25)
Clavicle ends	29 (15–46)	0.14 (31)	0.8 (25)
Scapula	22 (9–47)	0.24 (42)	0.96 (23)
Sternum	15 (8–22)	0.15 (29)	1.4 (9)
Cervical vertebrae	21 (16–28)	0.14 (14)	0.15 (10)
Thoracic vertebrae	14 (7–19)	0.12 (17)	0.6 (15)
Lumbar vertebrae + Sacrum	14 (7–19)	0.12 (17)	0.6 (15)

Table prepared by the authors based on their own data [25]

Note: parentheses contain the coefficient of variation (CV, %); for *BV/TV*, the range of possible values is provided; *Tb. Th.* — trabecular thickness, *Tb. Sp.* — mean trabecular separation, *BV/TV* — bone volume fraction.

Table 3. Linear dimensions and cortical bone layer thickness for basic phantoms of bone segments of 15-year-old male and female adolescents

Hematopoietic site	Segment	Shape[1]	Sex	Phantom parameters, mm (parenthetic CV, %)[2]					
				h	*a*	*b*	*c*	*d*	*Ct. Th.*
Femur	Neck	cyl	m	29.6 (5)	36 (14)	32 (13)	–	–	1.9 (19)
			f	30.5 (5)	29.4 (14)	23.9 (13)	–	–	1.9 (19)
	Trochanter area	dc	m	41 (4)	66 (6)	44 (6)	30 (7)	30 (7)	2.3 (15)
			f	34.5 (5)	58 (7)	39 (7)	27 (6)	27 (6)	2.3 (15)
Humerus	Proximal end	dc	m	28 (12)	56 (5)	56 (5)	19.4 (4)	19.4 (4)	1.1 (16)
			f	24.9 (12)	51.3 (5)	51.3 (5)	19.4 (4)	19.4 (4)	1.1 (16)
Ribs	Ribs[4] 1–2	p	m+f	17 (12)	30	7 (14)	–	–	0.7 (38)
	Ribs[4] 11–12	p	m+f	11 (18)	30	6 (17)	–	–	0.7 (38)
	Ribs[4] 3, 4, 9, 10	p	m+f	13 (8)	30	7 (14)	–	–	1.2 (38)
	Ribs[4] 5, 6, 7, 8	p	m+f	14 (14)	30	8 (13)	–	–	0.7 (38)
Sacrum	Body-1	p	m	30 (7)	40 (11)	24.5 (10)	–	–	1.2 (35)
			f	30 (9)	37.8 (11)	22.2 (12)	–	–	1.2 (35)

Table 3 (continued)

Hematopoietic site	Segment	Shape[1]	Sex	Phantom parameters, mm (parenthetic CV, %)[2]					
				h	*a*	*b*	*c*	*d*	*Ct. Th.*
Sacrum	Body-2-3	p	m	46 (8)	28.7 (11)	15 (9)	–	–	1.2 (35)
			f	45.2 (15)	28 (11)	13.8 (13)	–	–	1.2 (35)
	Body-4-5	p	m	36 (9)	28 (11)	8 (13)	–	–	1.2 (35)
			f	35 (14)	28 (11)	8.5 (12)	–	–	1.2 (35)
	Pedicle 1	cyl	m+f	13.9 (14)	23.7 (15)	15.3 (11)	–	–	1.2 (35)
	Pedicle 2	cyl	m+f	14.2 (14)	25 (11)	13.6 (17)	–	–	1.2 (35)
	Pedicle 3	cyl	m+f	13.9 (14)	18.3 (11)	13.2 (14)	–	–	1.2 (35)
	Pedicle 4	cyl	m+f	13.9 (14)	14.5 (11)	11.2 (18)	–	–	1.2 (35)
	Ala 1	p	m	30 (13)	20 (10)	42 (13)	–	–	1.2 (35)
			f	30 (9)	21 (15)	38.6 (8)	–	–	1.2 (35)
	Ala 2	p	m	26 (15)	23 (17)	25 (8)	–	–	1.2 (35)
			f	26 (9)	23 (17)	22.7 (13)	–	–	1.2 (35)
	Ala 3–4	pr	m+f	19 (16)	18 (9)	38.5 (15)	38.5 (15)	–	1.2 (35)
Pelvic bones	Iliac ala	p	m+f	9.5 (31)	30	30	–	–	1 (30)
	Iliac crest	p	m	11 (15)	30	13 (9)	–	–	1 (30)
			f	11 (15)	30[6]	13 (9)	–	–	1 (30)
	Iliac dorsal segment	p	m+f	19 (16)	30	30	–	–	1 (30)
	Ischium ramus	cyl	m+f	30[6]	34 (9)	25 (8)	–	–	0.5 (30)
	Pubis ramus inferior	dc	m+f	47 (17)	16 (25)	22 (23)	26 (23)	14 (36)	0.5 (30)
	Pubis ramus superior (lower part)	p	m	32 (19)	15 (20)	29 (20)	–	–	0.7 (30)[4] 1.5 (12)[4]
			f	31 (13)	14 (7)	33 (18)	–	–	0.7 (30)[4] 1.5 (12)[4]
	Pubis ramus superior (upper)	p	m	51.2 (8)	14.5 (20)	16 (20)	–	–	0.7 (30)[4] 1.5 (12)[4]
			f	83 (7)	11 (18)	16 (20)	–	–	0.7 (30)[4] 1.5 (12)[4]
	Acetabulum	hc	m+f	29 (10)	26 (10)	21 (20)	–	–	0.5 (30)[5] 3.6 (30)[5]
Skull	Flat bones[4]	p	m+f	5.2 (12)	30[6]	30[6]	–	–	1.3 (33)[3] 1.5 (22)[3]
Clavicle	Shaft (acromial part)	cyl	m	19.8 (5)	22 (9)	12 (29)	12 (17)	12 (8)	0.8 (26)
			f	20.7 (9)	21 (6)	10 (32)	10 (9)	10 (10)	0.8 (26)
	Body	dc	m	30	12 (17)	12 (8)	–	–	1.8 (2)
			f	30	10 (9)	10 (10)	–	–	1.8 (2)

Table 3 (continued)

Hematopoietic site	Segment	Shape[1]	Sex	Phantom parameters, mm (parenthetic CV, %)[2]					
				h	*a*	*b*	*c*	*d*	*Ct. Th.*
Clavicle	Shaft (sternal part)	dc	m	19.8 (5)	26 (15)	24 (13)	12 (17)	12 (8)	0.8 (26)
			f	20.7 (9)	24 (16)	21 (14)	10 (9)	10 (10)	0.8 (26)
Scapula	Glenoid	cyl	m+f	16.9 (8)	30.7 (11)	22.3 (18)	–	–	0.9 (28)
	Acromion	p	m+f	8.8 (18)	32.4 (4)	25.2 (4)	–	–	0.8 (13)
	Lateral margin	p	m+f	30	3.5 (3)	10 (12)	–	–	0.8 (13)
Sternum	Body	p	m+f	10.6 (14)	30	30	–	–	0.9 (44)
Cervical vertebrae	Vertebral body 3–7	cyl	m+f	11.9 (11)	15.2 (8)	19 (14)	–	–	0.3 (7)
	Vertebral body 2	p	m+f	19.2 (13)	14.3 (10)	17.5 (3)	–	–	0.3 (7)
	Lateral mass 1	p	m+f	15 (13)	11.4 (9)	10.5 (9)	–	–	0.3 (7)
Thoracic vertebrae	Vertebral body	cyl	m+f	18.6 (16)	28.7 (19)	24.9 (20)	–	–	0.4 (25)
	Lamina+inferior articular. proc.	p	m+f	32 (12)	10.2 (14)	4.2 (13)	–	–	1.3 (16)
	Spinous process	p	m+f	9.3 (18)	33 (18)	4.9 (18)	–	–	0.4 (25)
	Superior articular process	p	m+f	11.4 (12)	11.3 (14)	4.4 (11)	–	–	1.3 (16)
	Transverse process	p	m+f	9.9 (18)	14.8 (18)	8.6 (19)	–	–	0.4 (25)
Lumbar vertebrae	Vertebral body	cyl	m+f	24.7 (12)	31.5 (8)	44.5 (9)	–	–	0.4 (25)
	Lamina+inferior articular. proc.	p	m+f	20.4 (10)	12.7 (13)	4.1 (13)	–	–	1.0 (34)
	Spinous process	p	m+f	24 (10)	31 (10)	5.6 (10)	–	–	0.4 (25)
	Superior articular process	p	m+f	14 (14)	15 (13)	12 (17)	–	–	1.0 (34)
	Transverse process	p	m+f	10.7 (10)	20.5 (11)	5.6 (10)	–	-[6]	0.4 (25)

Table prepared by the authors based on their own data [25, 36]

Note: m — male; f — female; m+f — BPS was modeled independent of sex; [1] — phantom shape was designated as follows: cyl — cylinder, dc — deformed cylinder, p — rectangular parallelepiped, pr — prism with triangle base; t — hollow cylinder; [2] — BPS dimensions were designated as follows: *h* — height; *a* — major axis (c), major axis for a large base (dc) or side a (p) or outer diameter (t); *b* — minor axis (c), minor axis for a large base (dc) or side b (p) or inner diameter (t); *c* — major axis for a small base (dc); *d* — minor axis for a small base (dc); for prism(pr): *a, b, c* — sides of the triangle base; [3] — cortical layer thickness was assumed to be different for the inner (medial) and outer (gluteal) surfaces of a given segment of the skull; [4] — symphyseal surface covered by thicker cortical layer than other surfaces of BPS; [5] — a higher *Ct. Th*. value assumed for the medial side of the acetabulum; [6] — BPS imitated only a part of the simulated bone segment, when the bone segment dimensions exceeded significantly 30 mm, since in terms of dosimetry in such cases it makes no sense to simulate the entire bone fragment; "–" — dimension is not used for constructing the phantom of this segment.

adolescents are presented in Table 3. The data sources used to obtain these parameters are presented in [24].

Unlike bone microstructural parameters, the linear dimensions of several bones depend on sex; therefore, their dimensions were estimated separately for males and females. The SPSD phantoms of the skeleton for 15-year-old male and female adolescents consist of 46 BPSs, of which 14 segments are specific to males, another 14 are specific to females, and 32 segments were modeled identically for both sexes, as shown in Table 3. The sacrum was the most segmented skeletal region with active hematopoiesis. It comprised 10 BPSs, while a single BPS was used to model both the humerus and the skull.

The basic phantoms of bone segments (BPS) for a 15-year-old adolescent are mostly shaped as cylinders or rectangular parallelepipeds. Their dimensions ranged 3.5–66 mm. Sexual dimorphism is characteristic of many BPSs, with the greatest differences observed in the inferior part of the superior pubic ramus, at the level of 66%. The cortical bone layer of the modeled phantoms ranged from 0.3 mm (cervical vertebral bodies) to 2.3 mm (proximal end of the femur). *BV/TV* varied 12–52%, trabecular thickness ranged 0.1–0.29 mm, and the trabecular separation was 0.45–1.4 mm (Table 4).

The population variability of individual linear phantom dimensions ranged from 3% (cervical vertebral bodies) to 36% (inferior pubic ramus), with an average of 30% across all dimensions of all BPSs. The greatest variability in the cortical bone layer thickness was estimated for the sternum — 44%, while the smallest was for the cervical vertebral bodies — 3%. On average, the variability of *Ct.Th.* was 27%. For microarchitecture parameters, this indicator ranged from 6% to 42%. The volume of the generated SPSs ranged 23–264% of the BPS volume.

DISCUSSION

We used approximately 100 literature sources describing bone samples (> 5000) from 4592 individuals [24] to estimate the parameters of phantoms for 15-year-old male and female adolescents. A total of 197 parameters characterizing linear dimensions and 138 parameters characterizing the microstructure of the skeletal bones were evaluated to construct these phantoms. As mentioned earlier, some parameters for the phantoms of 15-year-old male and female adolescents were set equal to those for adults, specifically microarchitecture parameters for the clavicle, ribs, scapula, skull, cervical vertebrae, and sternum, as well as linear dimensions for the femoral neck, humerus, pelvic bones, and ribs.

By the age of 15, ossification processes are complete in many skeletal regions, and these regions were modeled using the same set of segments as for adults, although with different parameters. These include the femur, humerus, pelvic bones, sacrum, skull, ribs, and scapula. On the other hand, some skeletal regions modeled for adults were not modeled for 15-year-olds, such as the articular processes and arches of the thoracic and lumbar vertebrae. Consequently, the skeletal phantom for 15-year-old male and female adolescents consists of a smaller number of segments than adult phantoms, but a greater number than phantoms for younger children.

The RBM distribution in 15-year-olds is similar to that in adults; however, the RBM fraction in the vertebrae is greater in adults than in 15-year-olds, while the RBM fraction in the femur and humerus is, conversely, smaller.

The *BV/TV* for the BPS of 15-year-olds averages 20%, which is slightly higher than that for adults (17.3%). Age-related changes in *Tb. Th.* are insignificant, whereas *Tb. Sp.* for 15-year-olds is 18% lower than for adults. Table 4 presents a comparison of the media volumes within the BPS for 15-year-old male and female adolescents, as well as for adult males and females.

Table 4. Comparison of the basic phantoms of bone segment volumes for a 15-year-old child and adult men and women

BPS	Modeled media	Volume of modeled structure, cm^3			
		Adults		15-year-old child	
		Male	Female	Male	Female
Femur neck	BM	18.43	10.39	13.6	7.92
	TB	3.68	2.14	7.38	4.31
	CB	5.94	4.58	5.8	4.62
	Entire BPS	28.05	17.11	25.35	16.85
Proximal humerus	BM	32.26	24.2	23.9	18.36
	TB	2.02	1.54	6.27	4.82
	CB	3.47	3.14	3.54	2.95
	Entire BPS	37.75	28.88	33.71	26.13
First sacral vertebra (S1) body	BM	21.87	18.37	23.07	19.53
	TB	3.84	3.24	3.55	3.1
	CB	3.70	3.47	2.79	2.55
	Entire BPS	29.41	25.08	29.41	25.18

Table prepared by the authors based on their own data [25, 36]

Note: BM — bone marrow; CB — cortical bone; TB — trabecular bone; BPS — basic phantoms of bone segments.

Due to their smaller linear dimensions, the total volume of the BPS for 15-year-old adolescents is 21% less than that for adults. The sexual dimorphism in the average BPS volumes was 11%, and for individual segments, it reached 73% (ribs 11–12).

CONCLUSION

The present work is the sixth in a series of articles devoted to the parameters of computational skeletal phantoms for humans of different ages and sexes. In this article, we provide a description of SPSD phantoms of the skeleton for 15-year-old male and female adolescents. The phantoms consist of 46 BPSs. For 14 out of the 46 segments, sexual dimorphism in linear dimensions was taken into account.

Based on the assessment of parameter variability, 12 SPSs were generated for each BPS. The DF calculated for the SPSs will be used to assess their population variability.

The generated phantoms can be applied for the internal dosimetry of bone-seeking beta-emitters in the population, as well as for the dosimetry of other beta-emitting radionuclides, including those used in radionuclide therapy, such as ^{89}Sr, ^{32}P, ^{186}Re, ^{188}Re, and ^{117m}Sn.

Further research will focus on DF calculating, as well as on developing computational phantoms for the internal dosimetry of bone-seeking radionuclides during the intrauterine period.

References

1. Krestinina LY, Epifanova S, Silkin S, Mikryukova L, Degteva M, Shagina N, et al. Chronic low-dose exposure in the Techa River Cohort: risk of mortality from circulatory diseases. *Radiation ang Environmental Biophysics*. 2013;52(1):47–57. https://doi.org/10.1007/s00411-012-0438-5
2. Akleyev AV. *Chronic radiation syndrome among residents of the Techa River riverside villages*. Chelyabinsk: Book; 2012 (In Russ.).
3. Preston DL, Sokolnikov ME, Krestinina LY, Stram DO. Estimates of Radiation Effects on Cancer Risks in the Mayak Worker, Techa River and Atomic Bomb Survivor Studies. *Radiation Protection Dosimetry*. 2017;173(1–3):26–31. https://doi.org/10.1093/rpd/ncw316
4. Spiers FW, Beddoe AH, Whitwell JR. Mean skeletal dose factors for beta-particle emitters in human bone. Part I: volume-seeking radionuclides. *The British Journal of Radiology*. 1978;51(608):622–7. https://doi.org/10.1259/0007-1285-51-608-622
5. Degteva MO, Napier BA, Tolstykh EI, Shishkina EA, Shagina NB, Volchkova AY, et al. Enhancements in the Techa River Dosimetry System: TRDS-2016D Code for Reconstruction of Deterministic Estimates of Dose from Environmental Exposures. *Health Physics*. 2019;117(4):378–87. https://doi.org/10.1097/HP.0000000000001067
6. O'Reilly SE, DeWeese LS, Maynard MR, Rajon DA, Wayson MB, Marshall EL, et al. An image-based skeletal dosimetry model for the ICRP reference adult female–internal electron sources. *Physics in Medicine and Biology*. 2016;61(24):8794–824. https://doi.org/10.1088/1361-6560/61/24/8794
7. Xu XG, Chao TC, Bozkurt A. VIP-Man: an image-based whole-body adult male model constructed from color photographs of the Visible Human Project for multi-particle Monte Carlo calculations. *Health Physics*. 2000;78(5):476–86. https://doi.org/10.1097/00004032-200005000-00003
8. Shah AP, Bolch WE, Rajon DA, Patton PW, Jokisch DW. A paired-image radiation transport model for skeletal dosimetry. *Journal of Nuclear Medicine*. 2005;46(2):344–53.
9. Hough M, Johnson P, Rajon D, Jokisch D, Lee C, Bolch W. An image-based skeletal dosimetry model for the ICRP reference adult male–internal electron sources. *Physics in Medicine and Biology*. 2011;56(8):2309–46. https://doi.org/10.1088/0031-9155/56/8/001
10. Bolch WE, Eckerman, K, Endo A, Hunt JGS, Jokisch DW, Kim CH, et al. ICRP Publication 143: Paediatric Reference Computational Phantoms. *Annals of the ICRP*. 2020;49(1):5–297.
11. Degteva MO, Tolstykh EI, Shishkina EA, Sharagin PA, Zalyapin VI, Volchkova AY, et al. Stochastic parametric skeletal dosimetry model for humans: General approach and application to active marrow exposure from bone-seeking beta-particle emitters. *PLOS One*. 2021;16(10):e0257605. https://doi.org/10.1371/journal.pone.0257605
12. Sharagin PA, Shishkina EA, Tolstykh EI. Computational red bone marrow dosimetry phantom of a one-year-old child enabling assessment of exposure due to incorporated beta emitters. *Extreme Medicine*. 2023;24(4):74–82 (In Russ.). https://doi.org/10.47183/mes.2022.045
13. Sharagin PA, Shishkina EA, Tolstykh EI. Computational red bone marrow dosimetry phantom of a one-year-old child enabling assessment of exposure due to incorporated beta emitters. *Extreme Medicine*. 2023;25(3):44–55 (In Russ.). https://doi.org/10.47183/mes.2023.030
14. Sharagin PA, Tolstykh EI, Shishkina EA. Computational phantom for a 5-year old child red bone marrow dosimetry due to incorporated beta emitters. *Extreme Medicine*. 2023;25(4):86–97 (In Russ.). https://doi.org/10.47183/mes.2023.061
15. Sharagin PA, Tolstykh EI, Shishkina EA. Computational phantom for the dosimetry of the red bone marrow of a 10-year-old child due to incorporated beta-emitters. *Extreme Medicine*. 2024;26(2):38–48 (In Russ.). https://doi.org/10.47183/mes.2024.032
16. Sharagin PA, Tolstykh EI, Shishkina EA. Computational phantom for red bone marrow dosimetry in adult males and females. *Extreme Medicine*. 2025;27(2):220–8 (In Russ.). https://doi.org/10.47183/mes.2025-286
17. Cristy M. Active bone marrow distribution as a function of age in humans. *Physics in Medicine and Biology*. 1981;26(3):389–400. https://doi.org/10.1088/0031-9155/26/3/003
18. Robinson RA. Chemical analysis and electron microscopy of bone. *Bone as a tissue*. New York: McGraw-Hill; 1960.
19. Vogler JB. 3rd, Murphy WA. Bone marrow imaging. *Radiology*. 1988;1683:679–93. https://doi.org/10.1148/radiology.168.3.3043546
20. Vande Berg BC, Malghem J, Lecouvet FE, Maldague B. Magnetic resonance imaging of the normal bone marrow. *Skeletal Radiology*. 1998;27:471–83. https://doi.org/10.1007/s002560050423
21. Vande Berg BC, Malghem J, Lecouvet FE, Maldague B. Magnetic resonance imaging of normal bone marrow. *European Radiology*. 1998;8(8):1327–34. https://doi.org/10.1007/s003300050547
22. Taccone A, Oddone M, Dell'Acqua AD, Occhi M, Ciccone MA. MRI "road-map" of normal age-related bone marrow.

II. Thorax, pelvis and extremities. *Pediatric Radiology*. 1995;25(8):596–606. https://doi.org/10.1007/bf02011826
23. Taccone A, Oddone M, Occhi M, Dell'Acqua AD, Ciccone MA. MRI «road-map» of normal age-related bone marrow. I. Cranial bone and spine. *Pediatric Radiology*. 1995;25(8):588–95. https://doi.org/10.1007/bf02011825
24. Tolstykh EI, Sharagin PA, Shishkina EA, Volchkova AYu, Smith MA, Napier BA. Stochastic parametric skeletal dosimetry model for human: anatomical-morphological basis and parameter evaluation. *PLOS One*. 2025;20(7):e0327156. https://doi.org/10.1371/journal.pone.0327156
25. Sharagin PA, Shishkina EA, Tolstykh EI, Volchkova AYu, Smith MA, Degteva MO. *Segmentation of hematopoietic sites of human skeleton for calculations of dose to active marrow exposed to bone-seeking radionuclides. Conference proceedings of sixth international conference on radiation and applications in various fields of research*. Macedonia; 2018. https://doi.org/10.21175/RadProc.2018.33
26. Shishkina EA, Sharagin PA, Volchkova AYu. Analytical Description of the Dose Formation in Bone Marrow due to 90Sr Incorporated in Calcified Tissues. *Radiation Safety Issues*. 2021;3:72–82 (In Russ.). EDN: LYGTKD
27. Valentin J. Basic anatomical and physiological data for use in radiological protection: reference values. *Annals of the ICRP*. 2002;32(3–4):1–277. https://doi.org/10.1016/S0146-6453(03)00002-2
28. Woodard HQ, White DR. The composition of body tissues. *British Journal of Radiology*. 1986;59:1209–18. https://doi.org/10.1259/0007-1285-59-708-1209
29. Shishkina EA, Timofeev YS, Volchkova AY, Sharagin PA, Zalyapin VI, Degteva MO, et al. Trabecula: A Random Generator of Computational Phantoms for Bone Marrow Dosimetry. *Health Physics*. 2020;118(1):53–9. https://doi.org/10.1097/hp.0000000000001127
30. Parisien MV, McMahon D, Pushparaj N, Dempster DW. Trabecular architecture in iliac crest bone biopsies: infra-individual variability in structural parameters and changes with age. *Bone*.1988;9(5):289–95. https://doi.org/10.1016/8756-3282(88)90012-9
31. Hazrati Marangalou J, Ito K, Taddei F, van Rietbergen B. Inter-individual variability of bone density and morphology distribution in the proximal femur and T12 vertebra. *Bone*. 2014;60:213–20. https://doi.org/10.1016/j.bone.2013.12.019
32. Van Dessel J, Huang Y, Depypere M, Rubira-Bullen I, Maes F, Jacobs R. A comparative evaluation of cone beam CT and micro-CT on trabecular bone structures in the human mandible. *Dento Maxillo Facial Radiology*. 2013;42(8):20130145. https://doi.org/10.1259/dmfr.20130145
33. Fanuscu MI, Chang TL. Three-dimensional morphometric analysis of human cadaver bone: microstructural data from maxilla and mandible. *Clinical Oral Implants Research*. 2004;15(2):213–8. https://doi.org/10.1111/j.1600-0501.2004.00969.x
34. Ibrahim N, Parsa A, Hassan B, van der Stelt P, Aartman IH, Nambiar P. Influence of object location in different FOVs on trabecular bone microstructure measurements of human mandible: a cone beam CT study. *Dento Maxillo Facial Radiology*. 2014;43(2):20130329. https://doi.org/10.1259/dmfr.20130329
35. Shishkina EA, Sharagin PA, Tolstykh EI, Smith MA, Napier BA, Degteva MO. Uncertainty of stochastic parametric approach to bone marrow dosimetry of ^{89,90}Sr. *Heliyon*. 2024;10(4):e26275. https://doi.org/10.1016/j.heliyon.2024.e26275
36. Sharagin PA, Shishkina EA, Tolstykh EI, Smith MA, Napier BA. Stochastic parametric skeletal dosimetry model for humans: Pediatric and adult computational skeleton phantoms for internal bone marrow dosimetry. *PLOS One*. 2025;20(7):e0327479. https://doi.org/10.1371/journal.pone.0327479

Authors' contributions. All the authors confirm that they meet the ICMJE criteria for authorship. The most significant contributions were as follows: Pavel A. Sharagin — acquisition, analysis and interpretation of data; drafting and revising the article; Evgenia I. Tolstykh — research methodology development; article revision; Elena A. Shishkina — research concept development; article revision.

Authors:

Pavel A. Sharagin, ORCID: https://orcid.org/0000-0002-1457-4916
Evgenia I. Tolstykh, Dr. Sci. (Biol.), ORCID: https://orcid.org/0000-0002-4958-3214
Elena A. Shishkina, Dr. Sci. (Biol.), ORCID: https://orcid.org/0000-0003-4464-0889